JCI insight

Tissue resident memory T cells contribute to protection against heterologous SARS-CoV-2 challenge

Abby Odle, … , Lok-Yin Roy Wong, Stanley Perlman

JCI Insight. 2024. https://doi.org/10.1172/jci.insight.184074.

Research In-Press Preview COVID-19 Virology

Widespread vaccination and natural infection have resulted in greatly decreased rates of severe disease, hospitalization and death after subsequent infection or reinfection with SARS-CoV-2. New vaccine formulations are based on circulating strains of virus, which have tended to evolve to more readily transmit human to human and to evade the neutralizing antibody response. An assumption of this approach is that ancestral strains of virus will not recur. Recurrence of these strains could be a problem for individuals not previously exposed to ancestral spike protein by vaccination or infection. Here, we addressed this question by infecting mice with recent SARS-CoV-2 variants and then challenging them with a highly pathogenic mouse-adapted virus closely related to the ancestral Wuhan-1 strain (SARS2-N501Y$_{MA30}$). We found that challenged mice were protected from death and substantial weight loss, even though they generally had low or no neutralizing antibody response to SARS2-N501Y$_{MA30}$ at the time of reinfection. T cell depletion from the previously infected mice did not diminish infection against clinical disease, although it did result in delayed kinetics of virus clearance in the nasal turbinate and in some cases, in the lungs. Levels of tissue resident memory T cells were significantly elevated in the nasal turbinate of previously infected mice compared to mice that had no previous exposure to SARS-CoV-2. However, this phenotype was not seen in […]

Find the latest version:

https://jci.me/184074/pdf

Tissue resident memory T cells contribute to protection against heterologous SARS-CoV-2 challenge

Abby Odle[1], Meenakshi Kar[2,3], Abhishek Verma[1], Alan Sariol[4], David K. Meyerholz[5], Mehul S. Suthar[2,3,6], Lok-Yin Roy Wong[1,7,8†] and Stanley Perlman[1†]

[1]Department of Microbiology and Immunology, University of Iowa, Iowa City, IA 52242, USA

[2]Center for Childhood Infections and Vaccines of Children's Healthcare of Atlanta, Department of Pediatrics, Emory University School of Medicine, Atlanta, GA 30322, USA

[3]Emory Vaccine Center, Atlanta, GA 30317, USA

[4]Department of Medicine, Washington University School of Medicine, St. Louis, MO 63110, USA

[5]Department of Pathology, University of Iowa, Iowa City, IA 52242, USA

[6]Department of Microbiology and Immunology, Emory University School of Medicine, Atlanta, GA 30329, USA.

[7]Department of Microbiology, Biochemistry and Molecular Genetics, Rutgers New Jersey Medical School, Newark, NJ 07103, USA

[8]Center for Virus-Host-Innate Immunity, Rutgers New Jersey Medical School, Newark, NJ, 07103, USA

† **Corresponding Authors:** Lok-Yin Roy Wong, PhD roy.wong@rutgers.edu and Stanley Perlman MD, PhD, Stanley-perlman@uiowa.edu

Abstract

New vaccine formulations are based on circulating strains of virus, which have tended to evolve to more readily transmit human to human and to evade the neutralizing antibody

response. An assumption of this approach is that ancestral strains of virus will not recur. Recurrence of these strains could be a problem for individuals not previously exposed to ancestral spike protein. Here, we addressed this by infecting mice with recent SARS-CoV-2 variants and then challenging them with a highly pathogenic mouse-adapted virus closely related to the ancestral Wuhan-1 strain (SARS2-N501Y$_{MA30}$). We found that challenged mice were protected from severe disease, despite having low or no neutralizing antibodies against SARS2-N501Y$_{MA30}$. T cell depletion from previously infected mice did not diminish infection against clinical disease, although it resulted in delayed virus clearance in the nasal turbinate and in some cases, in the lungs. Levels of tissue resident memory T cells were significantly elevated in the nasal turbinate of previously infected mice compared to naïve mice. However, this phenotype was not seen in lung tissues. Together, these results indicate that the immune response to newly circulating variants afforded protection against re-infection with the ancestral virus that was in part T cell based.

Introduction

SARS-CoV-2, the etiological agent of COVID-19, has evolved repeatedly since it first entered human populations in late 2019 (1, 2). Although the virus grew well in the human upper and lower respiratory tract at the time of its initial introduction, virus evolution took place over the next several months to enhance replication and transmission to susceptible individuals. Effective vaccines became widely available in December 2020. Vaccination, in conjunction with widespread infection, resulted in widespread immunity and selection for mutations in the virus that evaded the anti-virus antibody response, in addition to enhancing virus replication. Many of these variants contained greater than 20 mutations in the S protein (3, 4), leading to the hypothesis that evolution had occurred in

a persistently infected immunocompromised host (5–7), although this has not been proven.

Vaccines were originally formulated to induce a neutralizing antibody response against the ancestral virus strain (Wuhan-1) and studies in 2020-2021 showed that neutralizing antibody titers served as useful correlates of protection (8). As the virus has mutated, effective neutralizing antibody titers against the newest variants elicited by ancestral virus vaccines diminished several hundred-fold so that they are often undetectable (9–11). At the same time, serum neutralizing antibody titers against Wuhan-1 declined suggestive of a lack of durability (12, 13). Yet, even with this loss of the ability to neutralize the virus, humans are largely protected from hospitalization and death. These results suggest that other arms of the immune response, including the anti-virus T cell response, Fc receptor-dependent, non-neutralizing antibody function or the innate myeloid response contribute to protection (3, 14, 15).

At present, vaccine strategies involved eliciting a neutralizing antibody response against the circulating strain of SARS-CoV-2. For a short period of time, vaccines were bivalent and contained spike proteins from the Wuhan-1 and circulating (Omicron BA.1 or BA.5) strains. However, inclusion of the ancestral S protein induced a strong anamnestic immune response to antibody epitopes present in this strain, some of which were no longer expressed in the Omicron strains. Consequently, the ancestral S protein was removed from the latest vaccine formulations, which express a single Omicron S protein (XBB.1.5 JN.1 or KP.2). While there is little evidence that ancestral-like variants that formerly circulated in human populations have resurged, a concern is that re-emergence of these strains would cause significant disease in populations that have only been infected with, or vaccinated against more recent variants. Since SARS-CoV-2 has only been circulating briefly in human populations as compared to other viruses, the trajectory for its evolution is not well understood. Moreover, it has been reported that immunocompromised patients

78 are persistently infected by SARS-CoV-2 and harbor mutated virus (16). The presence of
79 diverse SARS-CoV-2 species poses a risk for re-emergence of ancestral-like variants.
80 To examine this possibility, we infected mice with Omicron variants and then
81 challenged with earlier strains. Unlike ancestral strains, nearly all of them, apart from the
82 B.1.617 (δ variant), can infect laboratory mice directly but disease is mild. Therefore, the
83 effects of prior infection or vaccination are usually addressed by assessing virus titers in
84 the lungs or nasal cavity (17, 18). In addition to measuring virus titers, we challenged mice
85 with a mouse-adapted virus derived from the Wuhan-1 strain (SARS2-N501Y$_{MA30}$) by
86 repeated passage through mouse lungs (19) . Mouse adaptation involved five changes in
87 the spike protein and 3 in nonstructural proteins. Of the five S protein mutations, four of
88 the five were present in all Omicron strains (K417N, E484K, Q498R, N501Y) whereas the
89 fifth mutation, Q493R, was present in a subset of Omicron variants. Moderate doses of
90 SARS2-N501Y$_{MA30}$ causes lethal disease in BALB/c mice of all ages and in C57BL/6 mice
91 greater than 3 months of age. Using mice initially infected with SARS-CoV-2 variants, we
92 found complete protection against clinical disease after challenge with SARS2-N501Y$_{MA30}$
93 in the absence of any detectable neutralizing antibody. These results were confirmed
94 using a virus reduction assay after challenge with the B.1.1.7 (α) variant, which was
95 present in human populations early in the pandemic and is able to infect mice directly.
96 SARS-CoV-2 specific T cells provided part, but not all of the protection afforded by prior
97 infection. Thus, prior infection with a recently circulating Omicron strain resulted in
98 protection against challenge with variants no longer in human populations, with protection
99 conferred by anti-virus T cells as well as immune mechanisms that require further
100 characterization.
101
102 **Results**

SARS-CoV-2 variants induce a neutralizing antibody response that wanes over time. Several previous studies reported the waning of SARS-CoV-2-specific neutralizing antibody titers following vaccination or infection, and significantly decreased neutralizing activity against new variants of concern (VOC) (20–23). We sought to not only evaluate the kinetics of the antibody response elicited by circulating variants after infection but also if these presently circulating strains afforded protection against SARS-CoV-2 strains present early in the pandemic. Our study was divided into four cohorts of C57BL/6 mice that were intranasally infected with high doses of either B.1.351 (β), BA.2.12.1, BA.5 or XBB.1.5 virus (**Figure 1A**). Sera were collected from mice at various days post infection (dpi) and titers against the homologous virus were measured. The neutralizing titers in each cohort against the corresponding variant, except those against B.1.351, were significantly reduced over time. B.1.351 is known to be more virulent in mice than other human strains, contributing to the enhanced immune response (24–26). The reduction was most pronounced for most variants between 20- and 60-dpi (**Figure 1C-E**). In contrast, B.1.351-infected mice showed modest increase in antibody response from 20- to 60-dpi (**Figure 1B**). Mice previously infected with BA.2.12.1 exhibited lower levels of neutralizing antibodies at 20 dpi relative to the other variants and had minimal neutralizing activity by 60 dpi (**Figure 1C**). Mice infected with BA.5 or XBB.1.5 had similar antibody levels, with average titers at 301 and 282, respectively, at 20 dpi (**Figure 1D-E, left**). Individual titers for each mouse were tracked over the course of the experiment. We found that XBB.1.5 titers waned from 20- to 60 days with minimal changes in titers from 60- to 100 days (**Figure 1E, right**). These data indicated that each variant was able to induce a neutralizing antibody response to the homologous virus, but peak neutralizing titers varied greatly by variant. Additionally, there was evidence of significant waning in neutralizing antibodies for each virus, apart from B.1.351, just two months after infection. However,

the rate of waning was much less pronounced 3+ months later. consistent with patterns of SARS-CoV-2 antibody decline described previously (27).

Infected mice are protected from reinfection with lethal SARS2-N501Y$_{MA30}$.

Next, we investigated if these mice would still be protected against a lethal dose of a mouse-adapted virus, SARS2-N501Y$_{MA30}$, 3 months post initial infection. Mice were reinfected with 5,000 PFU of SARS2-N501Y$_{MA30}$ and weight loss was measured during acute infection (**Figure 2A**). There was complete protection against death with minimal weight loss in mice infected with any of the variants as compared to control groups (**Figure 2B**). Mice previously infected with B.1.351 experienced the least amount of weight loss while mice previously infected with XBB.1.5 experienced the most, at approximately 10% loss. The same sera that were used to measure neutralizing titers against the homologous virus was also tested against SARS2-N501Y$_{MA30}$ to examine cross-reactivity. Sera were obtained prior to reinfection. We found strong neutralizing activity against SARS2-N501Y$_{MA30}$ in mice infected with B.1.351 with no significant difference in titer between 20- and 60 days post initial infection (**Figure 2C**). In contrast, previous infection with BA.5 and BA.2.12.1 elicited much lower neutralizing titers, with neutralizing titers undetectable at 60 dpi with BA.2.12.1. Mice previously infected with XBB.1.5 did not mount a detectable level of neutralizing antibodies against SARS2-N501Y$_{MA30}$ at any of the time points. These data indicate that there are factors contributing to protection against disease that did not involve neutralizing activity.

XBB.1.5 induces a robust S protein-specific antibody response.

Given the discrepancy between the clinical efficacy of prior infection with several VOCs and the lack of a neutralizing antibody response, we next assessed whether broad spectrum S protein binding activity could be detected after XBB.1.5 infection. For this

purpose, we measured IgG and IgA binding to SARS-CoV-2 spike proteins WA1, BA.1 and the homologous virus, XBB.1.5 in the sera, and in nasal turbinate and lung homogenates. We examined three different groups of mice: the 'original' group belonged to the same cohort of XBB.1.5 infected mice described above (**Figure 1E, Figure 2B-C**). These mice were infected at 4 months of age and sacrificed 3 months later. The 'aged' group were infected at 7 months of age with the XBB.1.5 variant and sacrificed 21 days later. The 'young' group were infected at 12 weeks and sacrificed at 15 weeks of age, 21 days following XBB.1.5 infection (**Figure 3A**). The highest antibody binding in the sera was found to be against XBB.1.5 in each cohort, as expected (**Figure 3B**). Levels of binding to XBB.1.5 were also found to be comparable between the cohorts despite the differences in both age and duration post infection. In contrast, antibody responses to the WA.1 and BA.1 variants were lower, with the lowest responses observed 21 days after XBB.1.5 infection of 7-month-old mice. SARS-CoV-2 IgG responses in the lungs and nasal turbinates paralleled those observed in the sera, although antibody binding to all of the variant S proteins was more equivalent in the nasal turbinates. Again, the highest antibody binding was against XBB.1.5 while the lowest levels were against BA.1 (**Figure 3C**).

Contrary to these results, we detected SARS-CoV-2-specific IgA in only a fraction of homogenates. WA.1-specific IgA responses were detected in the nasal turbinates at 21 days after XBB.1.5 infection, and in the lungs of young and aged mice (**Figure 3D**). Therefore, the complete protection of previously infected mice against subsequent lethal infection challenge despite the lack of detectable neutralizing antibodies against SARS2-$N501Y_{MA30}$ is likely conferred by antibody-dependent processes, such as Fc-mediated responses in addition to T cells.

Previously infected mice depleted of T cells have increased viral titers in nasal turbinates and to a lesser extent, lungs upon reinfection. $CD4^+$ and $CD8^+$ T cell

responses have been implicated in protection against SARS-CoV-2 infection in several studies (14, 28–33). We next assessed the role of the T cell response in mice previously infected with the BA.2.12.1 or XBB.1.5 variants and challenged with SARS2-N501Y$_{MA30}$. $CD4^+$ and $CD8^+$ T cells were depleted at the time of challenge. Depletion of T cells in the lung and nasal turbinate tissue was confirmed by flow cytometry, both in the vasculature (IV+) and the parenchyma (IV-) (**Figure S1A-C**). Mice were then assessed for weight loss, and lungs and nasal tissue were collected for measurement of viral titers (**Figure 2A**). Depletion of T cells was not found to influence survival during lethal infection since mice had 0% mortality regardless of the variant used for initial infection (**Figure 2B**). Weight changes largely mimicked those of non-depleted mice both in XBB.1.5 and BA.2.12.1-infected mice. Next, viral loads in the lungs and in the nasal turbinates were measured at 3- and 5 dpi (**Figure 4A**). Within the cohort of mice previously infected with BA.2.12.1, we found no difference in lung virus titers between non-depleted ('BA.2.12.1') and T cell depleted ('BA.2.12.1 Depleted') mice (**Figure 4B**). However, in the nasal turbinates, T cell depleted BA.2.12.1-infected mice were found to have significantly higher viral titers than the non-depleted group. Mice infected with B.1.351, which had the highest neutralizing antibody titers (**Figure 1B**) did not have detectable levels of infectious virus in the lungs at 3 days post challenge with SARS2-N501Y$_{MA30}$ (**Figure 4B**). Since neutralizing antibodies responses persisted in mice infected with B.1.351, T cell depletion assays were not performed using this virus. Mice previously infected with BA.5 virus showed a similar phenotype to BA.2.12.1-infected mice; T cell depleted mice and non-depleted mice had no differences in viral lung titers at 3- and 5 dpi (**Figure 4C**). Again, there were significantly higher viral titers in the nasal turbinates of T cell-depleted mice compared to the non-depleted group at 3 dpi..

To further explore the effect of T cells upon a second exposure to SARS-CoV-2, mice in the XBB.1.5 cohort were treated with α-$CD4^+$ or α-$CD8^+$ antibody, with both antibodies or not depleted at all prior to SARS2-$N501Y_{MA30}$ challenge. After prior infection with XBB.1.5 and T cell depletion, virus clearance in the lungs was diminished at 5 dpi. Mice that were depleted of $CD8^+$ or doubly depleted of $CD4^+$ and $CD8^+$ T cells exhibited higher SARS2-$N501Y_{MA30}$ lung titers than mice that were $CD4^+$ T cell or mock depleted (**Figure 4D**). Of note, BA.2.12.1-infected mice also exhibited a lack of neutralizing antibodies against SARS2-$N501Y_{MA30}$ at 60 dpi, and while the differences in lung titers between BA.2.12.1 T cell depleted mice and BA.2.12.1 mice were not found to be significant, those in BA.2.12.1-infected mice trended lower than those in the depleted group (**Figure 4B**).

We detected higher viral titers in the nasal turbinates of mice previously infected with XBB.1.5 after $CD4^+$/$CD8^+$ or $CD8^+$ T cell depletion compared to non-depleted mice (**Figure 4D**). This was most pronounced at 3 dpi, where titers in $CD4^+$ T cell-depleted mice closely resembled mice that were not depleted while titers in $CD8^+$ T cell depleted mice were similar to those detected in doubly depleted mice. As in XBB.1.5-infected mice, greater differences were observed in the nasal turbinates after T cell depletion in BA.2.12.1 mice (**Figure 4B**). Pathological examination of the lungs of mice previously infected with XBB.1.5 and then reinfected with SARS2-$N501Y_{MA30}$ showed high levels of edema and cellular infiltrates in the PBS group at 5 dpi (**Figure 4F**). In contrast, there was minimal evidence of tissue damage in both the non-depleted and T cell-depleted groups for XBB.1.5. However, T cell-depleted mice had decreased numbers of cellular infiltrates present as compared to mice in which these cells were not depleted, consistent with the absence of T cells.

To determine whether these results obtained after infection with SARS2-N501Y$_{MA30}$ (derived from the ancestral Wuhan-1 strain) were also observed after challenge with another early appearing variant, mice that were previously infected with XBB.1.5 were reinfected with the B.1.1.7 variant. Viral titers in the nasal turbinate of depleted mice were significantly higher at 5 dpi than mice that were not T cell-depleted (**Figure 4E**). Together these results suggest that there is a protective role for memory CD8$^+$ T cells in the response to subsequent virus infection, but also that they do not appear to be necessary for protection from clinical disease in mice.

Antigen experienced tissue resident memory T cells are increased in the nasal cavity of previously infected mice upon reinfection. These data suggest an important role for virus-specific memory CD8$^+$ T cells in the nasal turbinates, and to a lesser extent, in the lungs in reducing virus burden. To assess whether these cells can be detected at these sites of infection, we infected mice with XBB.1.5 and then subsequently reinfected them with 2,000 PFU SARS2-N501Y$_{MA30}$ 3 months later. Lungs and nasal turbinates were harvested 3 days post challenge. Virus specific CD8$^+$ T cells were assessed by MHC class I (H2-K^b) S539 tetramer staining. There was a significant increase in the frequency and numbers of tetramer S539-positive cells in the nasal turbinates and to a lesser extent in the lungs of SARS2-N501Y$_{MA30}$-challenged mice that had been previously infected with XBB.1.5 (**Figure 5A**). We additionally characterized this tetramer S539-positive population in the nasal turbinates and found that it largely consisted of tissue resident memory T cells (T_{RM}) identified by CD69$^+$CD103$^+$ staining. Given that these cells expressed T_{RM} markers, it is not likely that they originated in extranasal tissue. In addition, since mice were analyzed at 3 days post challenge, it is unlikely that they originated de novo from naïve T cell populations. Previously infected mice had a significant increase in tetramer S539$^+$ CD8$^+$ T_{RM} frequency and numbers in the nasal turbinates compared to the

PBS group, which was also significant in the lungs, though less pronounced (**Figure 5B**). Finally, the overall T_{RM} population between the PBS mice and the mice previously infected with XBB.1.5 did not differ in both the nasal turbinate and lung tissues (**Figure 5C**).

Discussion

As SARS-CoV-2 becomes endemic, the virus continued to mutate rapidly in response to immunity induced by vaccines and prior infections to generate antigenically distant variants replacing earlier strains. In response, vaccines were updated because early formulations were less effective against these new variants in terms of inducing neutralizing antibodies. One consequence of the changes in viruses and vaccines is that unvaccinated, uninfected individuals, including young children will not be exposed to past variants and therefore, may develop no immunity against such previous variants that are no longer circulating. Re-emergence of past variants may pose significant threats to future generations who have never been exposed to these original variants, as previously demonstrated for influenza A virus (IAV) infection. During the 2009 H1N1 outbreak, young people were disproportionately affected by infection, while those born before 1957 experienced the lowest rates of morbidity (34–37). This was largely attributed to the pre-existing cross-reactive H1N1 antibodies and cell-mediated immunity acquired from childhood infection (38, 39).

Here, we showed that previous infection with B.1.351/Omicron variants protected against severe disease in mice after challenge with SARS2-N501Y_{MA30}, a mouse-adapted SARS-CoV-2 strain closely resembling the ancestral strain, suggesting that infection with the more recent SARS-CoV-2 variants induced cross-protection against early variants. Similarly, immunization with mRNA vaccines encoding spike protein of the ancestral Wuhan-1 strain or prior infection with early SARS-CoV-2 variants protected against severe

disease after infection with B.1.351/Omicron variants (40, 41). Together, these data indicate that immunity induced by vaccination or infection with antigenically distant SARS-CoV-2 strains are sufficient to cross-protect against severe disease after heterologous SARS-CoV-2 infection.

Levels of neutralizing antibody were previously identified as correlates of protection in the period when original circulating variants were circulating (42, 43). However, neutralizing antibodies are not the sole mechanism of protection since vaccinated humans are protected against severe disease and hospitalization but not infection after exposure to Omicron variants. Similarly, we observed that mice infected with B.1.351/Omicron variants were almost completely protected against subsequent challenge with a lethal dose of SARS2-N510Y$_{MA30}$ (**Figure 2B**). This phenomenon was independent of the immunizing variant, even in conditions where the levels of neutralizing titers to homologous or heterologous virus were low (XBB.1.5-infected mice, **Figure 1E, 2C**), suggesting that other immune functions contributed to protection. One of these factors is the T cell response. We observed that depletion of T cells resulted in delayed virus clearance in the nasal turbinates and to a lesser extent, the lungs (**Figure 4C**), confirming the role of T cells in controlling infection. Consistent with the role of prior infection in the induction of this T cell response, we showed that many of these T cells were resident memory T cells (**Figure 5**). Similarly, memory CD4$^+$ and CD8$^+$ T are rapidly induced following SARS-CoV-2 infection of vaccinated individuals (44). In addition, studies have shown that repeated vaccination or infection with mismatched SARS-CoV-2 strains often result in immunological imprinting (45, 46), therefore potentially contributing to reduced vaccine efficacy or protection. However, the T cell response was much less affected by imprinting as T cell epitopes were only modestly changed in new SARS-CoV-2 variants (47). T cell targets are also more diverse with epitopes located in multiple viral proteins in addition to

S protein. Therefore, vaccine strategies specifically boosting T cell responses as previously suggested (48) will help compensate for immunological imprinting and limit the emergence of escape mutants.

While our data suggest that virus-specific tissue-resident memory T cells contributed to protection in both the lungs and nasal turbinates (**Figure 4 and 5**), T cells were required for virus elimination to a greater extent in the latter than in the lungs (**Figure 4**). Although we showed that the frequency and number of tissue-resident memory T cells were diminished after depletion (Figure S1C), a limitation of our study is that T_{RM} could not be selectively depleted. Therefore, determining the specific role of T_{RM} in mediating protection warrants further investigation. In addition, another limitation is that we used inbred mouse strains and mouse-adapted virus, which does not reflect the diversity of immune responses in humans. Furthermore, T cell depletion only resulted in increased viral burden without detectable changes in clinical disease (**Figure 2 and 4**). Protection could result from the presence of non-neutralizing SARS-CoV-2-specific IgGs in the lungs and nasal turbinates (49) (**Figure 3**). Other studies identified virus-specific IgA responses in the respiratory mucosa and the presence of long-lasting memory B cells after infection and vaccination (50–52), which also likely contributed to protection. We were not able to detect significant IgA antibodies in the nasal turbinates of infected mice, possibly because IgA was present at lower levels than IgG, or IgA assays were less sensitive.

Overall, we showed that infection in mice with recent SARS-CoV-2 variants protected against challenge with early variants, consistent with key roles for neutralizing antibody-independent functions in protection. Moreover, we demonstrated an important role for T cell-mediated protection in the upper airway which will inform the design of next generation of mucosal vaccines against coronavirus infections.

Methods

Sex as a biological variable.

Our preliminary study used infected male and female mice. Nearly identical results were obtained. We used only female mice for this study because they were slightly more resistant to SARS-CoV-2 infection.

Cells and virus

All SARS-CoV-2 variants were obtained from BEI Resources: B.1.351 (β variant, NR-55282), BA.2.12.1 (NR-56781), BA.5 (NR-58616), XBB.1.5 (NR-59104) and B.1.1.7 (α variant, NR-54971). Mouse-adapted SARS2-N501Y$_{MA30}$ was generated as described (19). B.1.1.7, B.1.351 and SARS2-N501Y$_{MA30}$ were propagated in Calu-3 2B4 cells while Omicron variants BA.2.12.1, BA.5 and XBB.1.5 were propagated in Vero-TMPRSS2 cells. Calu-3 2B4 cells were obtained from Dr. Chien-Te Kent Tseng at the University of Texas Medical Branch in Galveston and were grown in Dulbecco's modified Eagle's medium (DMEM, GIBCO) supplemented with 20% FBS. Vero-TMPRSS2 cells were obtained from Dr. Michael Diamond (Washington University, Saint Louis) and were grown in DMEM supplemented with 10% FBS and 5μg/mL of blasticidin. Vero hACE2-TMPRSS2 cells, obtained from Dr. Michael Diamond, were used for the foci reduction neutralization test (FRNT50) and focus forming assay (FFA) experiments (see below) and were cultured in DMEM supplemented with 10% FBS, 1M HEPES (GIBCO) and 10μg/mL puromycin.

SARS-CoV-2 variant infection and SARS2-N501Y$_{MA30}$ or B.1.1.7 challenge in mice

Female C57BL/6 mice were purchased from Charles River Laboratories. Mice were anaesthetized with ketamine–xylazine and infected intranasally with 10^5 PFU of the indicated virus. In some experiments, infected mice were monitored daily for 3-4 months

before subsequent challenge with 5,000 PFU of SARS2-N501Y$_{MA30}$ or 10^5 PFU B.1.1.7. After reinfection, mice were monitored for weight loss and clinical disease. In other experiments (**Figure 3**), 12-week-old ('young') and 7-month-old ('aged') mice were infected intranasally with 10^5 PFU of XBB.1.5 and monitored daily for 21 days before sacrifice. All experiments with SARS-CoV-2 were performed in a biosafety level 3 (BSL3) laboratory at the University of Iowa.

Viral titers

Infected, challenged mice were sacrificed at 3 or 5 dpi and perfused intracardially with 10mL of PBS. Lungs and nasal turbinates were harvested and homogenized in 1mL PBS. Samples were aliquoted and stored at -80°C. Titers were measured by focus forming assays (FFA) using Vero hACE2-TMPRSS2 cells. Cells were seeded in 96-well plates and inoculated in 10-fold serial dilutions with lung or nasal turbinate homogenates for 1 hour at 37°C, 5% CO_2, gently rocking every 10 min. Then, the inoculum was removed, and cells were overlaid with 1:1 mixture of 2.4% carboxymethylcellulose and DMEM containing 4% FBS. Cells were stained and foci were visualized as detailed below.

Foci reduction neutralization test (FRNT50)

FRNTs were used to measure the neutralizing antibody activity against the SARS-CoV-2 variants and mouse-adapted SARS2-N501Y$_{MA30}$ virus. Mice were anaesthetized by intraperitoneal injection of ketamine–xylazine. Blood was collected through retro-orbital bleed with a capillary tube (Fisher Scientific). Blood was allowed to clot at room temperature for 60 min before centrifugation. Sera were removed into a new tube and stored at -20°C. Serial dilutions of the sera were incubated with an equal volume of 90-100 foci of the indicated virus at 37°C for 1 hour. Subsequently, 50 μL of the mixture were added to confluent Vero hACE2-TMPRSS2 cells in 96-well plates and incubated at 37°C,

5% CO_2 for 1 hour. After incubation, the inoculum was removed and 100 μL of overlay (1:1 mixture of 2.4% carboxymethylcellulose and DMEM containing 4% FBS) was applied to each well. Plates were incubated at 37°C, 5% CO_2 for 24 hours. After, cells were fixed with 200 μL of 4% paraformaldehyde for 1 hour at room temperature. Fixative was removed and cells were washed then permeabilized with 0.75% Triton-X100 for 20 mins followed by incubation with primary rabbit monoclonal α-SARS-CoV nucleocapsid antibody (1:1000 for 1 hour at 37°C, Sino Biological). Cells were then washed and incubated in secondary rabbit HRP-conjugated IgG antibody (1:500 for 1 hour at 37°C, Biolegend). Foci were visualized by addition of KPL TrueBlue peroxidase substrate (Sera-care) for 10 min at room temperature. The log antibody concentration was plotted against the percentage of inhibition of each concentration and the IC50 was calculated using a nonlinear variable slope equation: Y = 100/(1+10^((LogIC50-X)xHillSlope).

Histopathology

Mice were anaesthetized by intraperitoneal injection of ketamine–xylazine and perfused with 10 mL PBS. Tissues were fixed in zinc formalin and then embedded in paraffin. For routine histology, tissue sections (~4 μm) were stained with hematoxylin and eosin (H&E), and examined by a boarded veterinary pathologist. For experiments in which mice were infected with SARS2-N501Y_{MA30}, lung tissues were examined in a post-examination method of masking to group assignment (53). Lung edema and cellular infiltrate scores were evaluated based on extent of distribution as previously performed (54). High resolution images were taken using a BX53 microscope, DP73 digital camera, and Cell Sens Dimension software (Olympus).

Antibody Binding Assay

Blood sera and tissue homogenates of lungs and nasal turbinates from XBB.1.5 infected mice were assessed for the presence of IgG and IgA antibodies targeting the SARS-CoV-2 WA1, BA.1 and XBB.1.5 spike proteins using the V-PLEX SARS-CoV-2 Panel 34 (Mouse IgG) kit and V-PLEX SARS-CoV-2 Panel 34 (Mouse IgA) kit (Meso Scale Discovery, #K15696U-4) following the instructions provided by the manufacturer (55). The only difference between the Wuhan-1 strain, used in most experiments herein, and WA1 strain is one amino acid change in ORF8 and 2 silent alterations (in ORF1a and ORF1b). Initially, antigen-specific plates were prepared by blocking with MSD blocker at room temperature and shaking at 700 rpm for 30 minutes. The samples were then diluted 1:500, 1:5,000, and 1:50,000 and placed on the plates for two hours at room temperature. Subsequently, SULFO-TAG conjugated Goat anti-Mouse IgG or IgA antibody was added to their respective plates. Next, the plates were rinsed with 1X MSD wash buffer, followed by addition of MSD Gold Read Buffer B to each well. Plates were washed three times with wash buffer after each stage. Optical densities were measured using an MSD plate reader, and the data were analyzed with Discovery Workbench software, version 4.0. Antibody levels were reported in arbitrary units per mL (AU/mL) specific to SARS-CoV-2.

T cell depletion

Mice were depleted of $CD4^+$ and/or $CD8^+$ T cells by intraperitoneal injection of 250 µg α-$CD4^+$ mouse antibody (clone GK1.5, Leinco Technologies) and/or 250 µg α-$CD8^+$ mouse antibody (clone 2.43, Leinco Technologies) in 250 µL. Mice received antibody at days -2, 0 and +2 relative to challenge with SARS2-$N501Y_{MA30}$.

Tetramer Staining

Previously infected mice and naïve (PBS) mice were infected with 2,000 PFU of SARS2-$N501Y_{MA30}$ and sacrificed at 3dpi. Lungs and nasal turbinates were perfused with 10 mL

PBS and then harvested. Preparation of cells was performed as previously described (56). In short, tissues were minced then digested in 1mg/mL collagenase D (Roche Diagnostics) and 0.1mg/mL DNase I (Roche Diagnostics) nutating at 37°C for 1 hour. Tissues were then filtered twice through 70 μM cell strainers and washed before counting and subsequent staining. Virus-specific T cells were detected using APC-conjugated H2-K^b S539 tetramers obtained from the National Institutes of Health Tetramer Facility (National Institute of Allergy and Infectious Disease MHC Tetramer Core Facility). Cells were stained with 5 μg/mL S539 tetramer for 30 min at 4°C. The following antibodies were used: CD16/CD32 (2.4G2), LIVE/DEAD fixable violet stain (Thermo Fisher), Super Bright Complete Staining Buffer (eBioscience), Thy 1.2 (30-H12, Biolegend), CD45 (30-F11, Biosciences), CD3 (145-2C11, Invitrogen), CD4 (GK1.5, BD Horizon), CD8a (53-6.7, BD Biosciences), CD11a (2D7, BD Biosciences), CD49a (Ha31/8, BD Biosciences), CD69 (H1.2F3, BD Biosciences) and CD103 (M290, BD Horizon). Data were collected using a Cytek Aurora spectral flow cytometer.

Intravenous (IV) exclusion

Prior to sacrifice (**Figure 5**), mice were treated with 2μg of PerCP-Cy5.5-conjugated Thy1.2 antibody by IV injection for 5 minutes. Mice were then processed as described above. Samples were analyzed by flow cytometry, Thy1.2+ populations were denoted “IV+” and Thy1.2- populations were denoted “IV-”. All data presented in **Figure 5** are analyzed on the Thy1.2- population.

Statistical analysis

Statistical analyses were performed using Graph Pad Prism version 10.2.3 software (GraphPad Software Inc., La Jolla, CA, USA). Statistical significance was determined by Mann Whitney U test, one-way ANOVA with Tukey’s test for multiple comparisons or log-

rank followed by Bonferroni's correction for multiple comparisons. A p-value of <0.05 was considered statistically significant. *P<0.05**,** **P<0.01, ***P<0.001,****P<0.0001.

Study approval

All animal studies were approved by the University of Iowa Animal Care and Use Committee and meet stipulations of the Guide for the Care and Use of Laboratory Animals.

Acknowledgements

This project has been funded in part with Federal funds from the National Institute of Allergy and Infectious Diseases, National Institutes of Health, Department of Health and Human Services, under Contract No. 75N93021C00016, 75N93021C00017, 75N93021C00014, and NIH grant (R01 AI129269) (SP), P51 OD011132 (Emory Primate Center) and R00 AI170996 (L.-Y.R.W). Schematics in Figures 1-4 were created using BioRender.com.

Data availability

The data supporting the findings of this study are documented within the paper and are available from the corresponding authors upon request. Values for all the data points represented in the graphs of this paper are available in Supporting Data Values.

Authors contribution

A.O., L.-Y.R.W., A.S., M.S., S.P. conceived the work and designed the experiments; A.O., L.-Y.R.W., M.K. and A.V. acquired the data; A.O., L.-Y.R.W., A.S., D.K.M., M.K., M.S., S.P. analyzed the data; A.O., L.-Y.R.W., and S.P. wrote the manuscript.

Conflict of interest

All authors declare no competing interests.

References

1. Markov PV, et al. The evolution of SARS-CoV-2. *Nat Rev Microbiol*. 2023;21(6):361–379.

2. Carabelli AM, et al. SARS-CoV-2 variant biology: immune escape, transmission and fitness. *Nat Rev Microbiol*. 2023;21(3):162–177.

3. Mannar D, et al. Altered receptor binding, antibody evasion and retention of T cell recognition by the SARS-CoV-2 XBB.1.5 spike protein. *Nat Commun*. 2024;15(1):1854.

4. Tegally H, et al. Emergence of SARS-CoV-2 Omicron lineages BA.4 and BA.5 in South Africa. *Nat Med*. 2022;28(9):1785–1790.

5. Weigang S, et al. Within-host evolution of SARS-CoV-2 in an immunosuppressed COVID-19 patient as a source of immune escape variants. *Nat Commun*. 2021;12(1):6405.

6. Clark SA, et al. SARS-CoV-2 evolution in an immunocompromised host reveals shared neutralization escape mechanisms. *Cell*. 2021;184(10):2605-2617.e18.

7. Marques AD, et al. SARS-CoV-2 evolution during prolonged infection in immunocompromised patients. *mBio*. 2024;15(3):e00110-24.

8. Goldblatt D, et al. Correlates of protection against SARS-CoV-2 infection and COVID-19 disease. *Immunol Rev*. 2022;310(1):6–26.

9. Liu J, et al. BNT162b2-elicited neutralization of B.1.617 and other SARS-CoV-2 variants. *Nature*. 2021;596(7871):273–275.

10. Third BNT162b2 Vaccination Neutralization of SARS-CoV-2 Omicron Infection. *N Engl J Med.* 2022;386(5):492-494.

11. Zou Jing, et al. Neutralization of BA.4–BA.5, BA.4.6, BA.2.75.2, BQ.1.1, and XBB.1 with Bivalent Vaccine. *N Engl J Med*. 2023;388(9):854–857.

12. Durability of Booster mRNA Vaccine against SARS-CoV-2 BA.2.12.1, BA.4, and BA.5 Subvariants. *N Engl J Med.* 2022;387(14):1329-1331.

13. Six-Month Follow-up after a Fourth BNT162b2 Vaccine Dose. *N Engl J Med.* 2022;387(22):2092-2094.

14. Ying B, et al. Mucosal vaccine-induced cross-reactive CD8+ T cells protect against SARS-CoV-2 XBB.1.5 respiratory tract infection. *Nat Immunol*. 2024;25(3):537–551.

15. Lee A, et al. BCG vaccination stimulates integrated organ immunity by feedback of the adaptive immune response to imprint prolonged innate antiviral resistance. *Nat Immunol*. 2024;25(1):41–53.

16. Li Y, et al. SARS-CoV-2 viral clearance and evolution varies by type and severity of immunodeficiency. *Sci Transl Med*. 2024;16(731):eadk1599.

17. Hoffmann M, et al. Omicron subvariant BA.5 efficiently infects lung cells. *Nat Commun*. 2023;14(1):3500.

18. Baz M, et al. SARS-CoV-2 Omicron BA.1 Challenge after Ancestral or Delta Infection in Mice - Volume 28, Number 11—November 2022 - Emerging Infectious Diseases journal - CDC. https://doi.org/10.3201/eid2811.220718.

19. Wong L-YR, et al. Eicosanoid signalling blockade protects middle-aged mice from severe COVID-19. *Nature*. 2022;605(7908):146–151.

20. Pérez-Alós L, et al. Modeling of waning immunity after SARS-CoV-2 vaccination and influencing factors. *Nat Commun*. 2022;13(1):1614.

21. Gaebler C, et al. Evolution of antibody immunity to SARS-CoV-2. *Nature*. 2021;591(7851):639–644.

22. Levin Einav G., et al. Waning Immune Humoral Response to BNT162b2 Covid-19 Vaccine over 6 Months. *N Engl J Med*. 2021;385(24):e84.

23. Seow J, et al. Longitudinal observation and decline of neutralizing antibody responses in the three months following SARS-CoV-2 infection in humans. *Nat Microbiol*. 2020;5(12):1598–1607.

24. Halfmann PJ, et al. SARS-CoV-2 Omicron virus causes attenuated disease in mice and hamsters. *Nature*. 2022;603(7902):687–692.

25. Rizvi ZA, et al. Omicron sub-lineage BA.5 infection results in attenuated pathology in hACE2 transgenic mice. *Commun Biol*. 2023;6(1):1–14.

26. Uraki R, et al. Characterization and antiviral susceptibility of SARS-CoV-2 Omicron BA.2. *Nature*. 2022;607(7917):119–127.

27. Srivastava K, et al. SARS-CoV-2-infection- and vaccine-induced antibody responses are long lasting with an initial waning phase followed by a stabilization phase. *Immunity*. 2024;57(3):587-599.e4.

28. Liu J, et al. CD8 T cells contribute to vaccine protection against SARS-CoV-2 in macaques. *Sci Immunol*. 2022;7(77):eabq7647.

29. Chandrashekar A, et al. Vaccine protection against the SARS-CoV-2 Omicron variant in macaques. *Cell*. 2022;185(9):1549-1555.e11.

30. Liu J, et al. Vaccines elicit highly conserved cellular immunity to SARS-CoV-2 Omicron. *Nature*. 2022;603(7901):493–496.

31. Kar M, et al. CD4+ and CD8+ T cells are required to prevent SARS-CoV-2 persistence in the nasal compartment. *BioRxiv Prepr Serv Biol*. 2024;2024.01.23.576505.

32. Lieber CM, et al. Efficacy of late-onset antiviral treatment in immune-compromised hosts with persistent SARS-CoV-2 infection. *BioRxiv Prepr Serv Biol*. 2024;2024.05.23.595478.

33. Fumagalli V, et al. Antibody-independent protection against heterologous SARS-CoV-2 challenge conferred by prior infection or vaccination. *Nat Immunol*. 2024;25(4):633–643.

34. Fisman David N., et al. Older Age and a Reduced Likelihood of 2009 H1N1 Virus Infection. *N Engl J Med*. 2009;361(20):2000–2001.

35. Xu R, et al. Structural Basis of Preexisting Immunity to the 2009 H1N1 Pandemic Influenza Virus. *Science*. 2010;328(5976):357–360.

36. Hospitalized Patients with 2009 H1N1 Influenza in the United States, April–June 2009. *N Engl J Med.* 2009;361(20):1935-1944.

571 37. Chowell Gerardo, et al. Severe Respiratory Disease Concurrent with the Circulation
572 of H1N1 Influenza. *N Engl J Med*. 2009;361(7):674–679.

573 38. Greenbaum JA, et al. Pre-existing immunity against swine-origin H1N1 influenza
574 viruses in the general human population. *Proc Natl Acad Sci*. 2009;106(48):20365–
575 20370.

576 39. Cross-Reactive Antibody Responses to the 2009 Pandemic H1N1 Influenza Virus. *N*
577 *Engl J Med.* 2009;361(20):1945-1952.

578 40. Ying B, et al. Boosting with variant-matched or historical mRNA vaccines protects
579 against Omicron infection in mice. *Cell*. 2022;185(9):1572-1587.e11.

580 41. Protection against Omicron from Vaccination and Previous Infection in a Prison
581 System. *N Engl J Med.* 2022;387(19):1770-1782.

582 42. Khoury DS, et al. Neutralizing antibody levels are highly predictive of immune
583 protection from symptomatic SARS-CoV-2 infection. *Nat Med*. 2021;27(7):1205–1211.

584 43. Feng S, et al. Correlates of protection against symptomatic and asymptomatic
585 SARS-CoV-2 infection. *Nat Med*. 2021;27(11):2032–2040.

586 44. Painter MM, et al. Prior vaccination promotes early activation of memory T cells and
587 enhances immune responses during SARS-CoV-2 breakthrough infection. *Nat Immunol*.
588 2023;24(10):1711–1724.

589 45. Johnston TS, et al. Immunological imprinting shapes the specificity of human
590 antibody responses against SARS-CoV-2 variants. *Immunity*. 2024;57(4):912-925.e4.

591 46. Park Y-J, et al. Imprinted antibody responses against SARS-CoV-2 Omicron
592 sublineages. *Science*. 2022;378(6620):619–627.

593 47. Choi SJ, et al. T cell epitopes in SARS-CoV-2 proteins are substantially conserved in
594 the Omicron variant. *Cell Mol Immunol*. 2022;19(3):447–448.

595 48. Moss P. The T cell immune response against SARS-CoV-2. *Nat Immunol*.
596 2022;23(2):186–193.

597 49. Tan TJC, et al. Evidence of antigenic drift in the fusion machinery core of SARS-
598 CoV-2 spike. *Proc Natl Acad Sci*. 2024;121(15):e2317222121.

599 50. Havervall S, et al. Anti-Spike Mucosal IgA Protection against SARS-CoV-2 Omicron
600 Infection. *N Engl J Med*. 2022;387(14):1333–1336.

601 51. Turner JS, et al. SARS-CoV-2 infection induces long-lived bone marrow plasma cells
602 in humans. *Nature*. 2021;595(7867):421–425.

603 52. Turner JS, et al. SARS-CoV-2 mRNA vaccines induce persistent human germinal
604 centre responses. *Nature*. 2021;596(7870):109–113.

605 53. Meyerholz DK, Beck AP. Principles and approaches for reproducible scoring of
606 tissue stains in research. *Lab Invest*. 2018;98(7):844–855.

607 54. Zheng J, et al. COVID-19 treatments and pathogenesis including anosmia in K18-
608 hACE2 mice. *Nature*. 2021;589(7843):603–607.

609 55. Edara VV, et al. Infection- and vaccine-induced antibody binding and neutralization
610 of the B.1.351 SARS-CoV-2 variant. *Cell Host Microbe*. 2021;29(4):516-521.e3.

56. Zhao J, Zhao J, Perlman S. De Novo Recruitment of Antigen-Experienced and Naive T Cells Contributes to the Long-Term Maintenance of Antiviral T Cell Populations in the Persistently Infected Central Nervous System1. *J Immunol*. 2009;183(8):5163–5170.

Figure legends

Figure 1. Neutralization against SARS-CoV-2 variants. Mouse neutralizing antibody titers against SARS-CoV-2 variants were measured over time using an $FRNT_{50}$ assay. (**A**) Schematic of intranasal mouse infection and sera collection. Variants included were B.1.351 (**B**), BA.2.12.1 (**C**), BA.5 (**D**) or XBB.1.5 (**E**). Naïve mice were uninfected. (**B**) B.1.351 n=10 and naïve n=5. (**C**) BA.2.12.1 n=7 and naïve n=5. (**D**) BA.5 n=32 and naïve n=5. (**E**) XBB.1.5 n=19 and naïve n=5. Antibody titers were determined by the highest antibody dilution that resulted in a 50% reduction in the number of foci. Average serum antibody titer is listed above each group. LOD (limit of detection) = 20 PFU. *P* values were measured by one-way ANOVA followed by Tukey's test for multiple comparisons.

Figure 2. Sequential infection of mice with SARS-CoV-2 VOCs followed by SARS2-$N501Y_{MA30}$. (**A**) 4-month-old (XBB.1.5) or 6-month-old (other SARS-CoV-2 variants) C57BL/6 mice were infected intranasally with SARS-CoV-2 variants or mock-infected and were challenged with a lethal dose of SARS2-$N501Y_{MA30}$ 3 months later. (**B**) Mice previously infected with B.1.351 (blue), BA.2.12.1 (orange) or XBB.1.5 (purple) or mock infected ("PBS") were assessed for weight loss and survival after SARS2-$N501Y_{MA30}$ challenge. In some experiments, T cells were depleted at the time of challenge ("depleted"). *B.1.351* data are from one experiment. PBS n=5 and B.1.351 n=4. *BA.2.12.1* data are from two independent experiments. PBS n= 9, PBS depleted n=4, BA.2.12.1 n=7 and BA.2.12.1 depleted n=5. *XBB.1.5* data are from two independent experiments. PBS

n=6, XBB.1.5 n=8 and XBB.1.5 depleted n=7. Red statistics denote PBS vs. XBB.1.5 depleted, black statistics denote PBS vs. XBB.1.5. *P* values were measured by log-rank followed by Bonferroni's correction for multiple comparisons. (**C**) Sera obtained prior to challenge were tested for SARS2-N501Y$_{MA30}$ neutralizing antibodies. B.1.351 (blue), BA.2.12.1 (orange), BA.5 (green) or XBB.1.5 (purple). B.1.351 n=7, BA.2.12.1 n=7, BA.5 n=32, XBB.1.5 =19 and naïve n=5/group. Antibody titers are determined by the highest antibody dilution that results in a 50% reduction in the number of foci. Average titer is listed above each group. LOD= 20 PFU. *P* values measured by Mann Whitney U test (BA.2.12.1 and B.1.351) or one-way ANOVA followed by Tukey's test for multiple comparisons (BA.5).

Figure 3. SARS-CoV-2-specific antibody binding in sera, and nasal and lung tissues. Mice were infected intranasally with 10^5 PFU of XBB.1.5. (**A**) Schematic detailing the timeline and cohorts used for the antibody binding experiments. Three different cohorts of mice were used in this experiment. Sera and nasal turbinate and lung tissues were harvested at the indicated times for the measurement of total antibody (**B**), IgG (**C**) and IgA (**D**) binding to WA1, BA.1 and XBB.1.5 full length spike proteins, as described in Materials and Methods. (**B**) Antibody binding in serum. (**C**) Nasal turbinate and lung tissue IgG (**C**) and IgA (**D**) binding. For each cohort, n=4. Data are from one experiment. All results were obtained prior to reinfection with SARS2-N501Y$_{MA30}$. *P* values were measured by one-way ANOVA followed by Tukey's test for multiple comparisons. LOD= 0.67.

Figure 4. Effect of T cell depletion on kinetics of virus clearance. 4-month-old (XBB.1.5) or 6-month-old (other SARS-CoV-2 variants) C57BL/6 mice were infected with the indicated SARS-CoV-2 variant and challenged with SARS2-N501Y$_{MA30}$ 3 months later.

(**A**) Schematic detailing experimental timeline. $CD4^+/CD8^+$ T cells were depleted at the indicated time points. Mice were initially infected with BA.2.12.1 (**B**), B.1.351 (**B**), BA.5 (**C**), or XBB.1.5 (**D**). PBS mice were mock infected and then challenged with SARS2-$N501Y_{MA30}$. (**B**) 'BA.2.12.1' and 'B.1.351' were non-T cell depleted mice. n= 4/group. Data represent one experiment. (**C**) 3 dpi: PBS n=8, 'BA.5' (non-T cell-depleted), n= (8 lungs, 10 NT), BA.5 Depleted n=9. 5dpi: PBS n=9, BA.5 n=10, BA.5 Depleted n=10. Data are from two independent experiments. (**D**) 'XBB.1.5' were non-T cell depleted mice. Mice were CD4 T cell, CD8 T cell or CD4/CD8 T cell depleted. Each group contained 7-8 mice, from two independent experiments. Data in (**B-D**) are shown as mean ± SEM. Each symbol represents data obtained from one mouse. **E**) XBB.1.5-infected mice were challenged with the B.1.1.7 (α variant). Virus titers in the lungs and nasal turbinates were measured at 5 dpi. Each group contained 4 mice. Data are from one experiment. (**F**) Lung pathology of XBB.1.5, XBB.1.5-T cell depleted, and PBS mice at 5 dpi. PBS n=10, XBB.1.5 n=9, and XBB.1.5- T cell depleted n=8. Evidence of edema are denoted (*) and cellular infiltrates are marked with arrows. H&E stain, bar =450 and 90 μm, top and bottom rows, respectively. All *P* values were measured by one-way ANOVA followed by Tukey's test for multiple comparisons.

Figure 5. Memory T cell characterization at 3 days after challenge. Mice were challenged with SARS2-$N501Y_{MA30}$ 3 months post XBB.1.5 infection. Mice were briefly treated with PerCP-Cy5.5-conjugated anti-Thy1.2 to label cells in the vasculature, as described in the Materials and Methods. Lungs and nasal turbinates were harvested for class I tetramer staining 3 days post reinfection and Thy1.2- cells were analyzed by flow cytometry. PBS lungs n=8, PBS NT n=7. XBB.1.5 lungs n=9, XBB.1.5 NT n=8. Data represent two independent experiments. *P* values determined by Mann-Whitney U test. (**A**) Frequency (left) and number (right) of S539 tetramer positive T cells gated on $CD8^+$ T

cell population. Representative plots for lungs (left) and nasal turbinates (right) are shown. (**B**) Frequency (left) and number (right) of virus-specific T_{RM} gated on S539 tetramer positive T cells. Representative plots for lungs (left) and nasal turbinates (right) are shown. (**C**) Frequency (left) and number (right) of total T_{RM} gated on $CD8^+$ T cell population. Representative plots for lungs (left) and nasal turbinates (right) are shown.

Supplemental Figure 1. Depletion of $CD4^+$ and $CD8^+$ T cells in the lungs and nasal turbinates. Mice were administered α-$CD4^+$/$CD8^+$ antibody by IP injection at days -2, 0 and +2 relative to reinfection. Five minutes before lungs and nasal turbinates were harvested, mice received PerCP-Cy5.5-conjugated anti-Thy1.2 antibody by retroorbital injection. $CD4^+$ (A), $CD8^+$ (B) and $CD69^+CD103^+$ (C) T cells were measured by flow cytometry, distinguishing between cells in the vasculature (IV+) or the parenchyma (IV-). For each group n=5. *P* values were calculated by Mann-Whitney U test. Frequency (top row) and number (bottom) of $CD4^+$ or $CD8^+$ T cells are shown.

Supplemental Figure 2. Gating strategy for $S539^+$ tetramer and tissue resident memory T cell populations. Gating strategy shown using lung (A) or nasal turbinate (B) tissue from a mouse previously infected with XBB.1.5, 3 days post reinfection with SARS2-$N501Y_{MA30}$. PerCP-Cy5.5-conjugated Thy 1.2 antibody was used for IV labeling. The Thy1.2- population was subsequently analyzed.

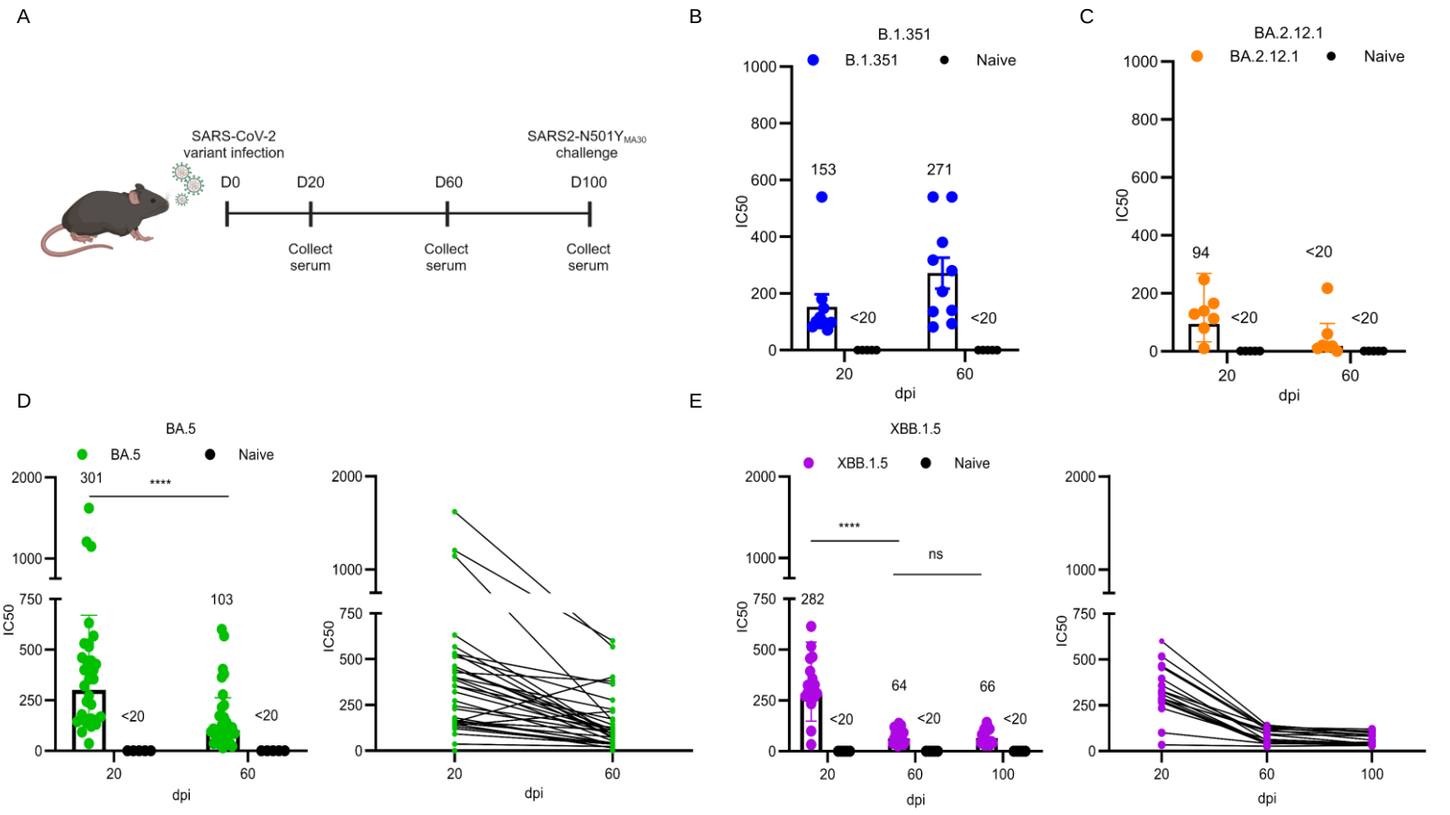
A
SARS-CoV-2
variant infection
SARS2-N501Y$_{MA30}$
challenge
D0
D20
D60
D100
Collect
serum
Collect
serum
Collect
serum
B
B.1.351
B.1.351
Naive
IC50
153
271
<20
<20
20
60
dpi
C
BA.2.12.1
BA.2.12.1
Naive
IC50
94
<20
<20
<20
20
60
dpi
D
BA.5
BA.5
Naive
301
****
103
<20
<20
IC50
20
60
dpi
E
XBB.1.5
XBB.1.5
Naive
****
ns
282
64
66
<20
<20
<20
IC50
20
60
100
dpi

Figure 1

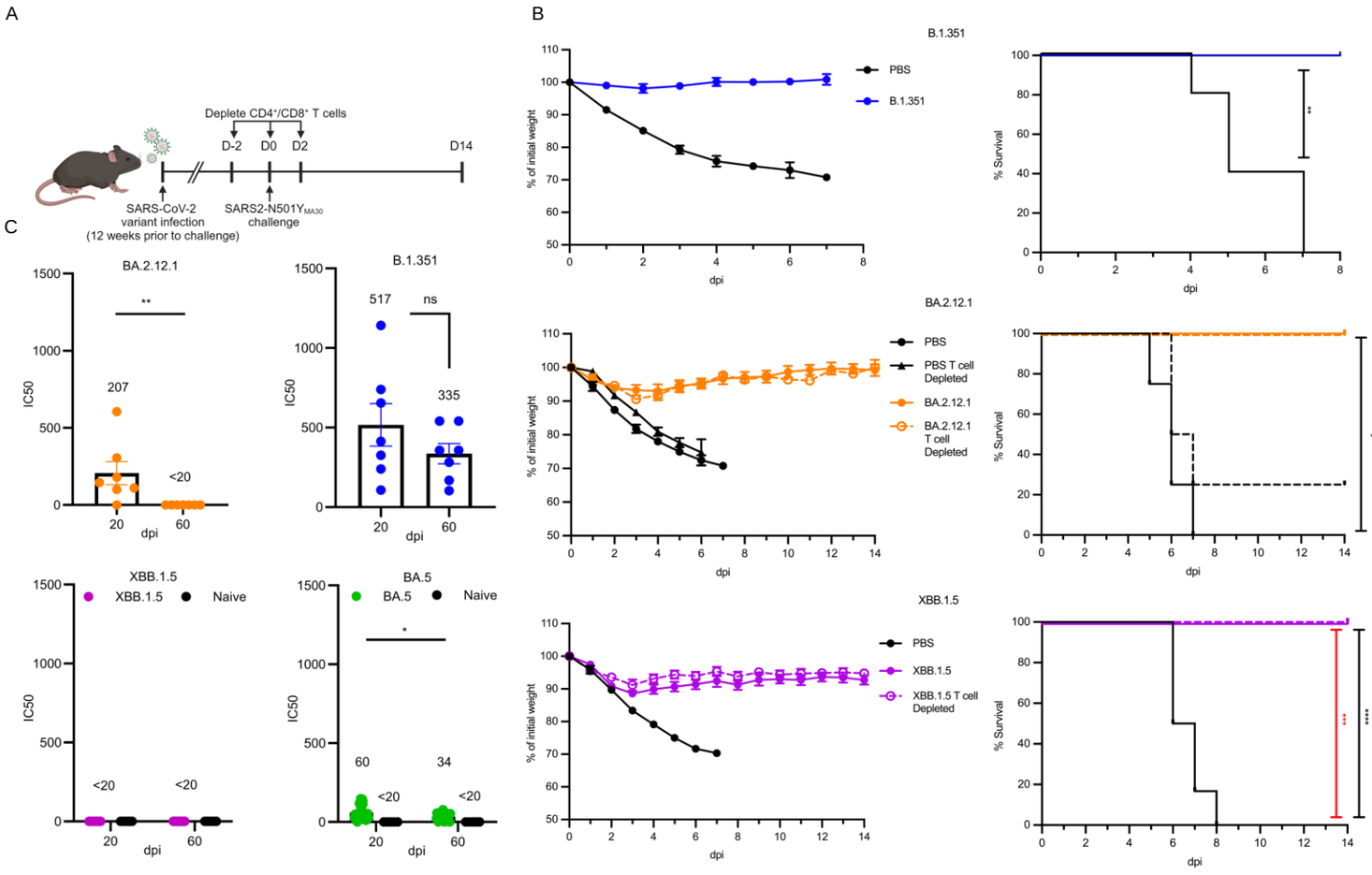
A
Deplete CD4+/CD8+ T cells
D-2
D0
D2
D14
SARS-CoV-2 variant infection (12 weeks prior to challenge)
SARS2-N501YMA30 challenge
B
B.1.351
PBS
B.1.351
% of initial weight
dpi
% Survival
BA.2.12.1
PBS
PBS T cell Depleted
BA.2.12.1
BA.2.12.1 T cell Depleted
XBB.1.5
PBS
XBB.1.5
XBB.1.5 T cell Depleted
C
BA.2.12.1
B.1.351
XBB.1.5
BA.5
Naive
IC50
dpi
207
<20
517
335
60
34
ns
**
*

Figure 2

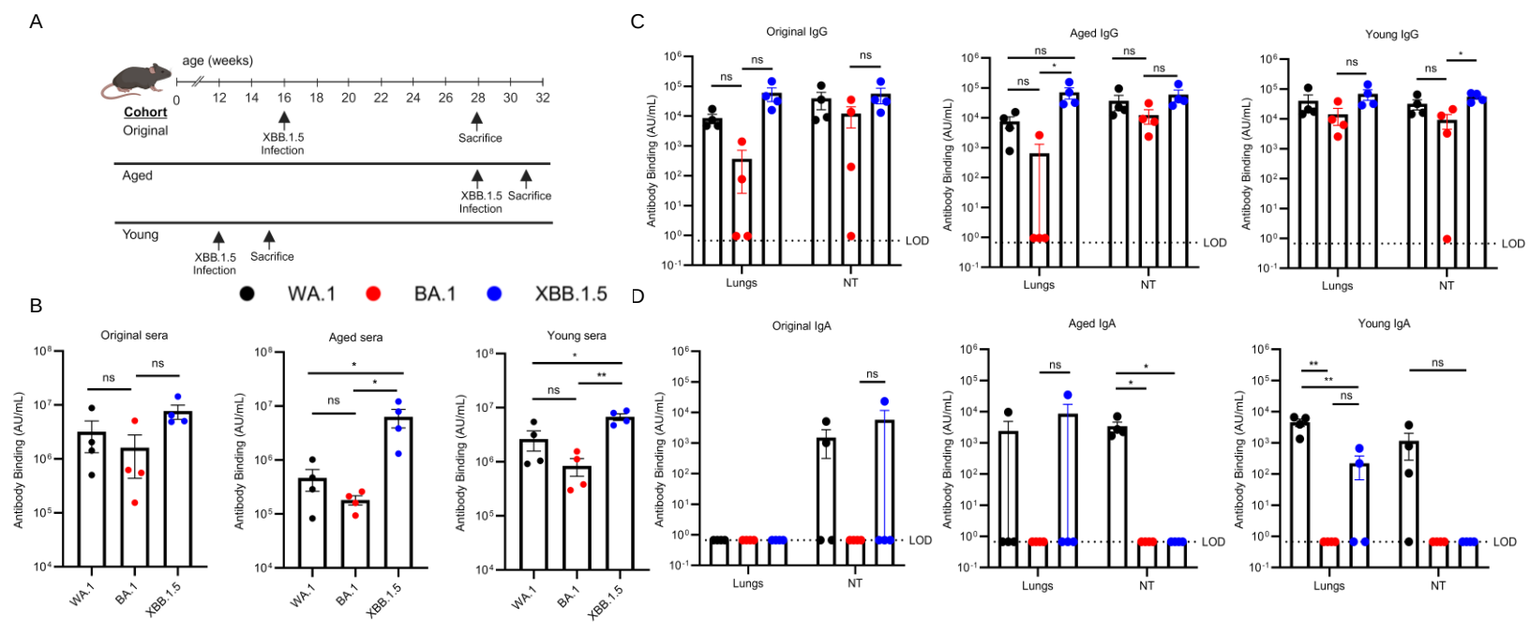
A
age (weeks)
0
12
14
16
18
20
22
24
26
28
30
32
Cohort
Original
XBB.1.5 Infection
Sacrifice
Aged
XBB.1.5 Infection
Sacrifice
Young
XBB.1.5 Infection
Sacrifice
WA.1
BA.1
XBB.1.5
B
Original sera
Aged sera
Young sera
Antibody Binding (AU/mL)
ns
*
**
WA.1
BA.1
XBB.1.5
C
Original IgG
Aged IgG
Young IgG
Antibody Binding (AU/mL)
LOD
Lungs
NT
D
Original IgA
Aged IgA
Young IgA
Antibody Binding (AU/mL)
LOD
Lungs
NT

Figure 3

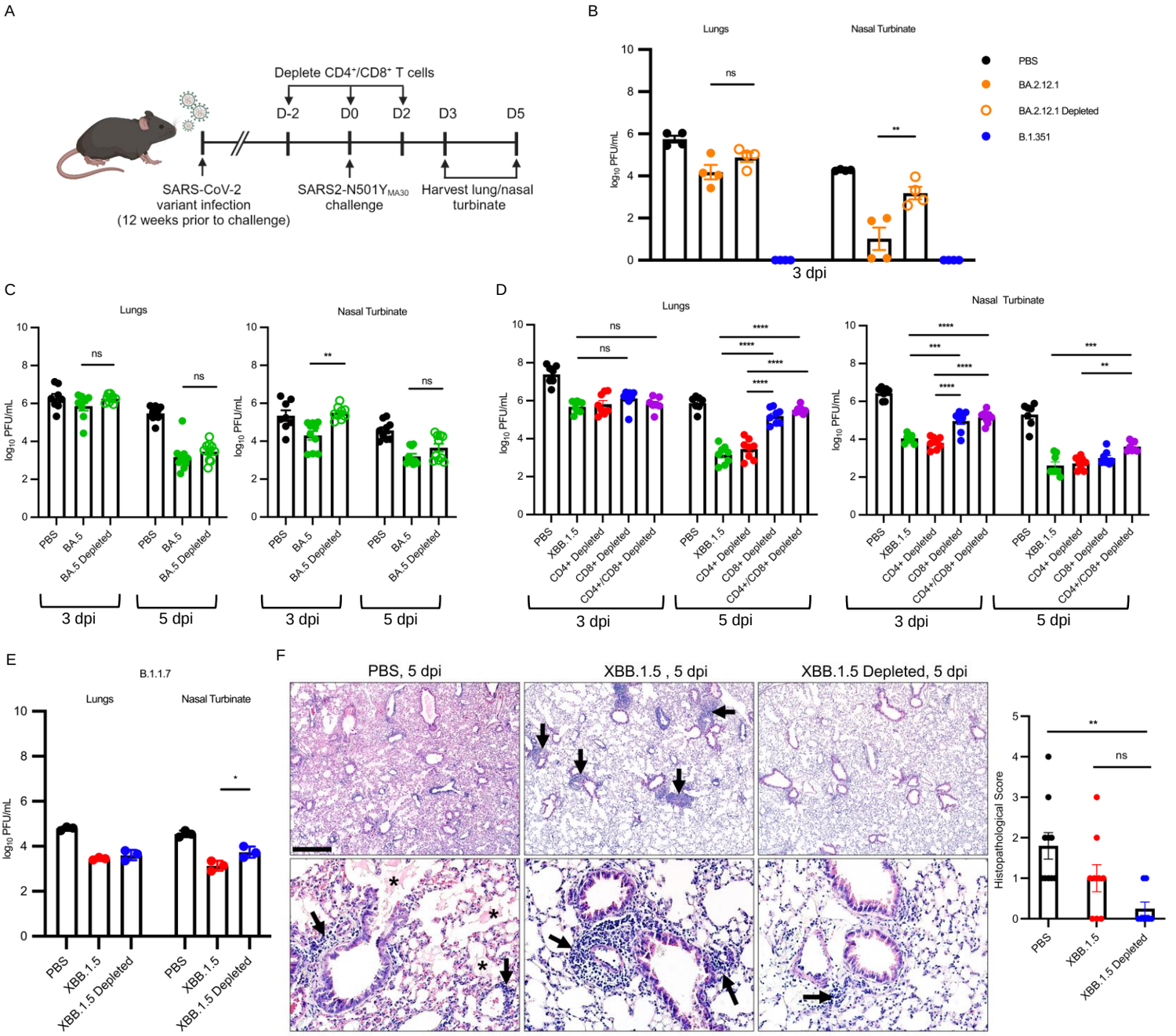
A
Deplete CD4+/CD8+ T cells
D-2
D0
D2
D3
D5
SARS-CoV-2 variant infection (12 weeks prior to challenge)
SARS2-N501YMA30 challenge
Harvest lung/nasal turbinate
B
Lungs
Nasal Turbinate
log10 PFU/mL
ns
**
PBS
BA.2.12.1
BA.2.12.1 Depleted
B.1.351
3 dpi
C
Lungs
Nasal Turbinate
log10 PFU/mL
ns
**
PBS
BA.5
BA.5 Depleted
3 dpi
5 dpi
D
Lungs
Nasal Turbinate
log10 PFU/mL
ns
****
***
**
PBS
XBB.1.5
CD4+ Depleted
CD8+ Depleted
CD4+/CD8+ Depleted
3 dpi
5 dpi
E
B.1.1.7
Lungs
Nasal Turbinate
log10 PFU/mL
*
PBS
XBB.1.5
XBB.1.5 Depleted
F
PBS, 5 dpi
XBB.1.5 , 5 dpi
XBB.1.5 Depleted, 5 dpi
Histopathological Score
**
ns
PBS
XBB.1.5
XBB.1.5 Depleted

Figure 4

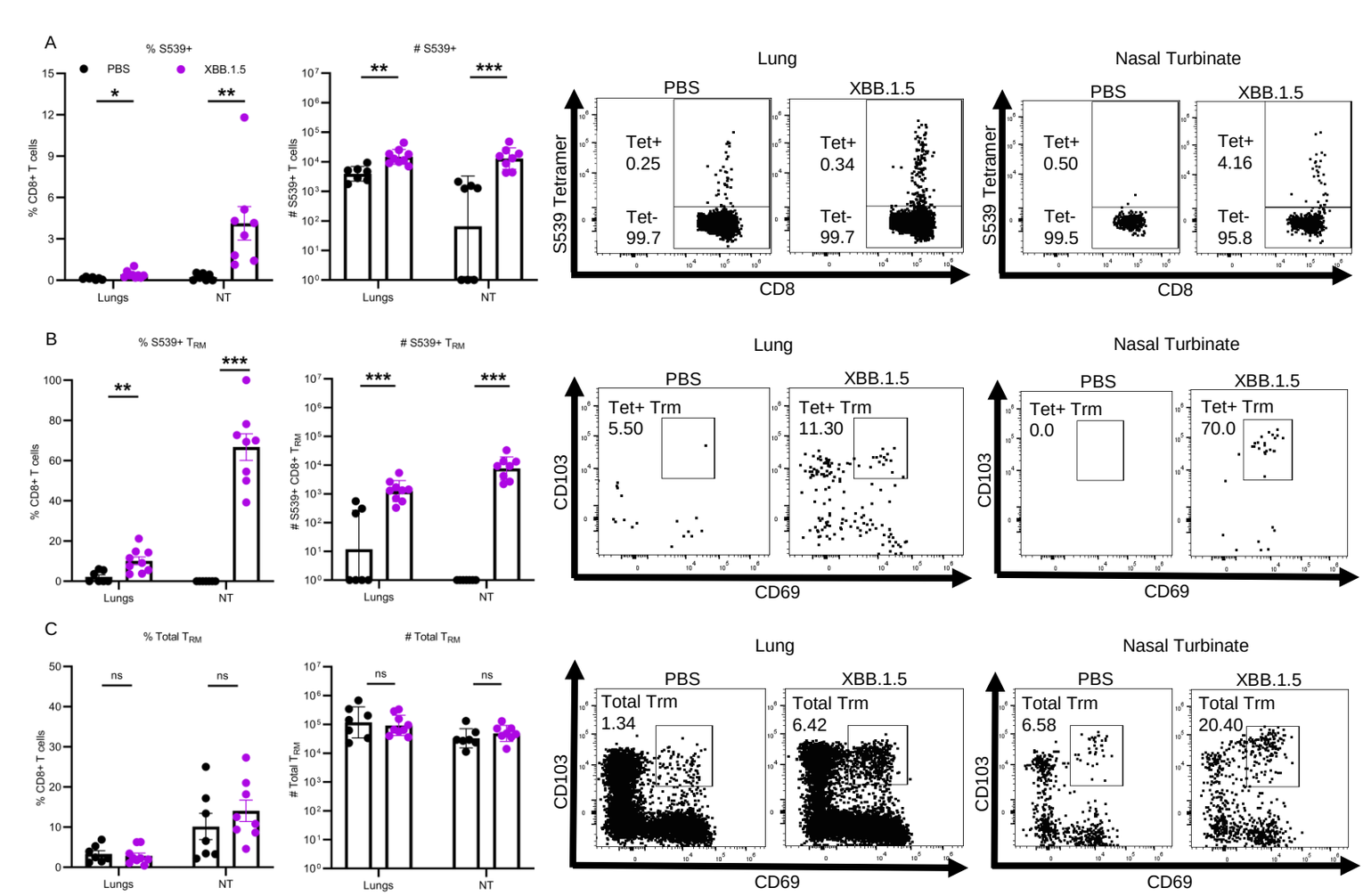
A
% S539+
PBS
XBB.1.5
% CD8+ T cells
Lungs
NT
S539+
S539+ T cells
Lung
Nasal Turbinate
S539 Tetramer
CD8
Tet+ 0.25
Tet- 99.7
Tet+ 0.34
Tet- 99.7
Tet+ 0.50
Tet- 99.5
Tet+ 4.16
Tet- 95.8
B
% S539+ TRM
# S539+ TRM
# S539+ CD8+ TRM
CD103
CD69
Tet+ Trm 5.50
Tet+ Trm 11.30
Tet+ Trm 0.0
Tet+ Trm 70.0
C
% Total TRM
# Total TRM
# Total TRM
ns
Total Trm 1.34
Total Trm 6.42
Total Trm 6.58
Total Trm 20.40

Figure 5

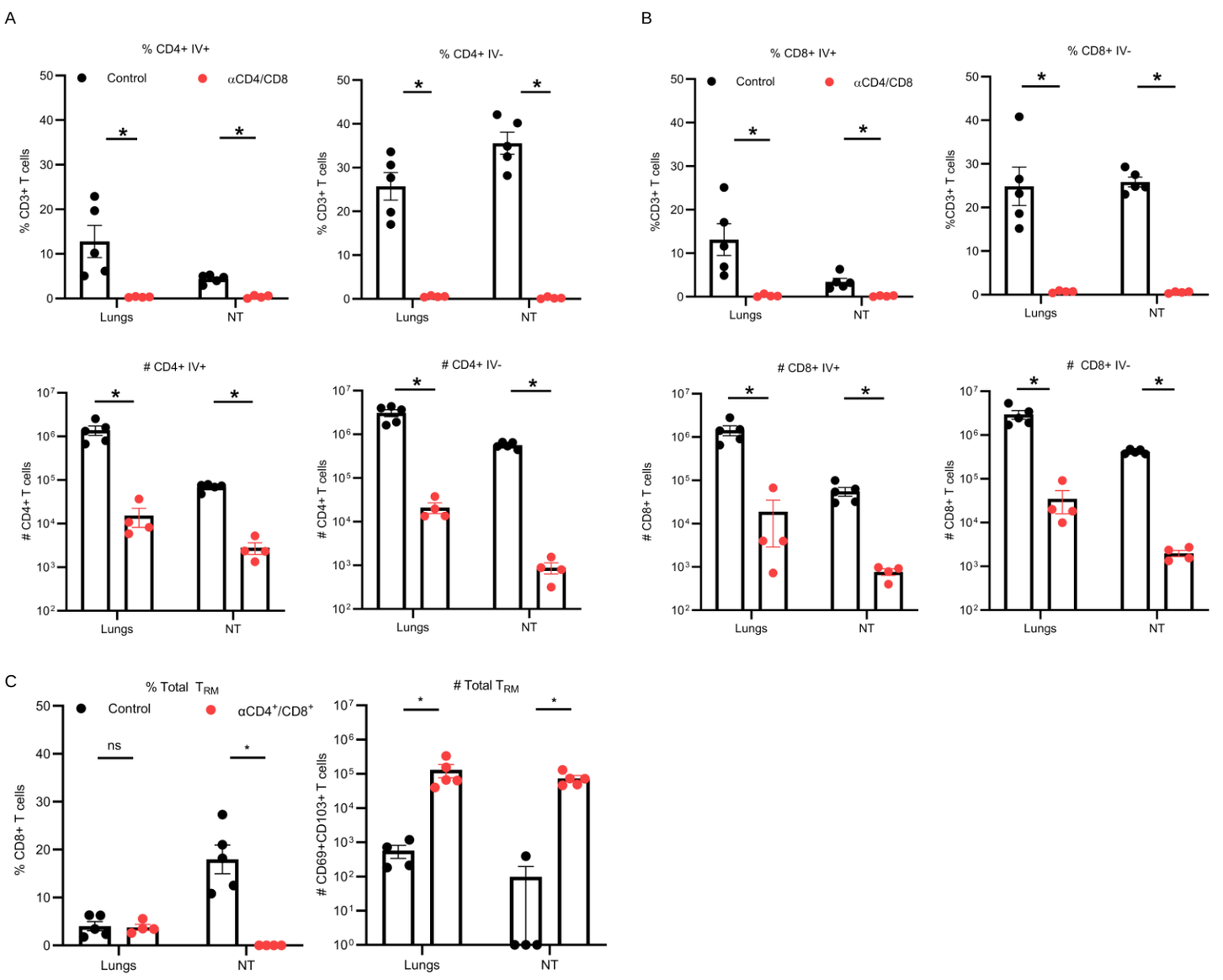

Supplemental Figure 1

A

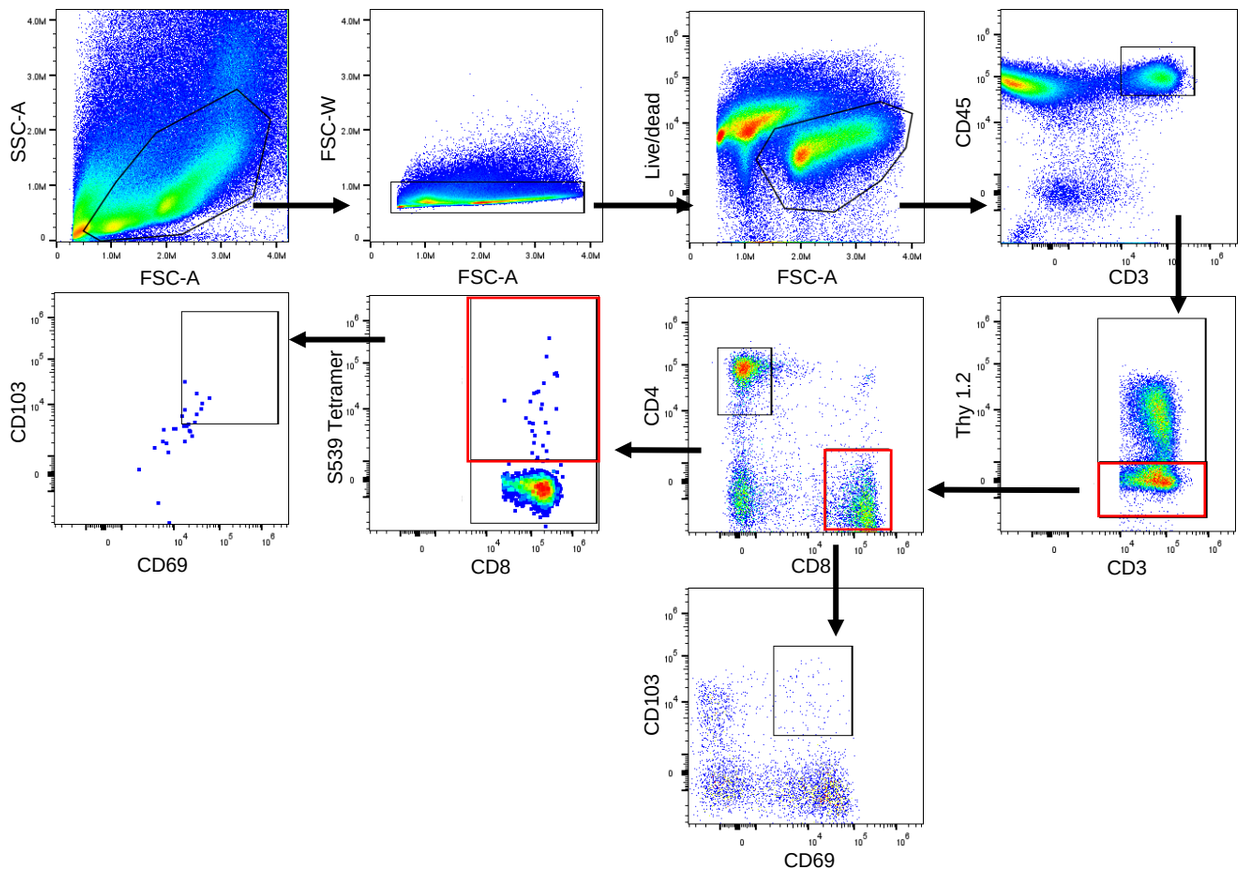

B

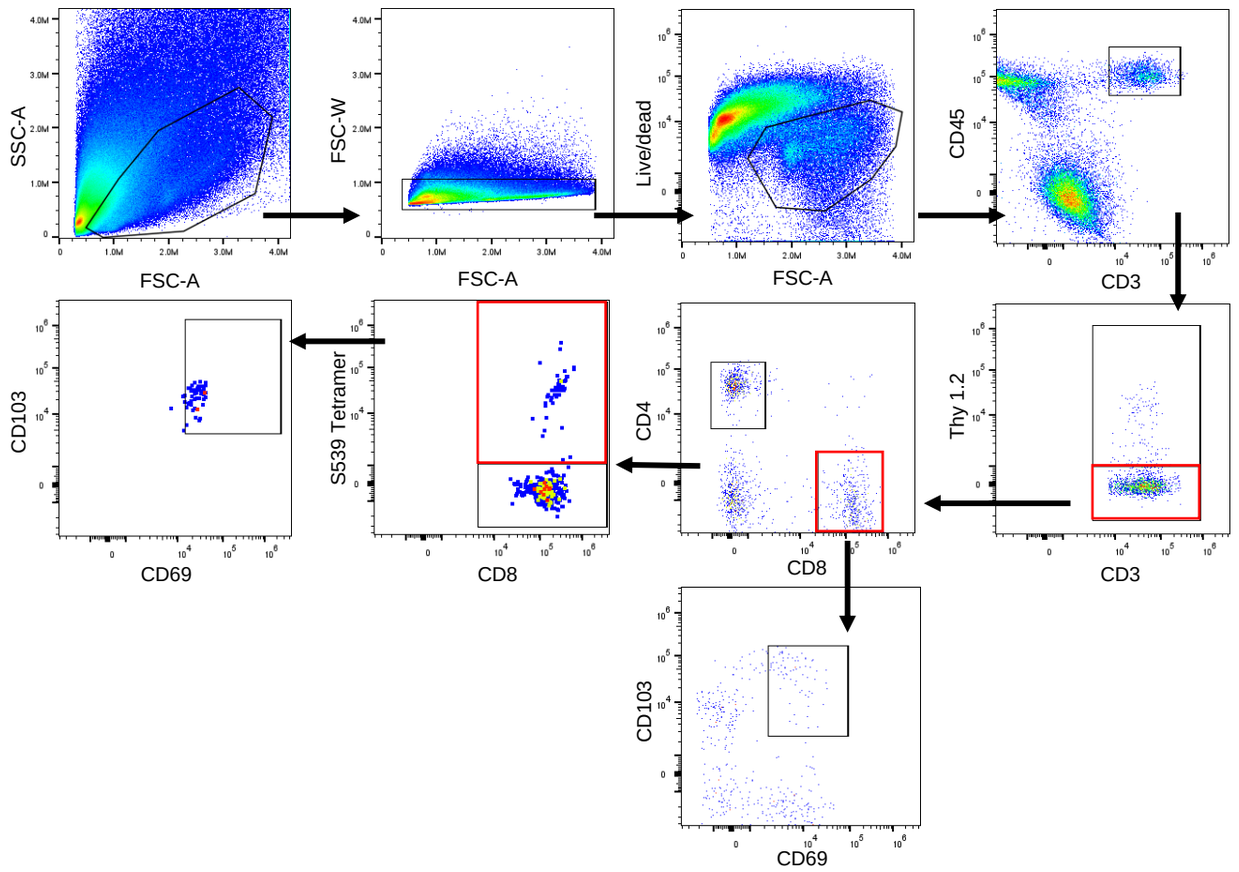

Supplemental Figure 2